# Analysis of ADCP data above a bottom observatory

**Jean-Luc Fuda** ([1]), **Claude Millot** ([1]), **Sven Hoog** ([2]) **and Hans W. Gerber** ([3])
([1]) *Laboratoire d'Océanographie et de Biogéochimie (LOB), La Seyne-sur-Mer, France*
([2]) *Institute of Naval Architecture and Ocean Engineering, Technical University of Berlin, Germany*
([3]) *TFH Berlin – University of Applied Sciences, Berlin, Germany*

**Abstract**
A 300-kHz ADCP was set on GEOSTAR, a six-m$^3$ deep-sea observatory. It was operated with cells of 80 cm during a three-week test experiment at 42-m water depth in the Northern Adriatic sub-basin. Although it provided valuable data on the horizontal current field over most of the water column, it also specified the wake disturbances induced by the observatory. These disturbances are characterised by vertical velocities that are significant up to ~20 m above seafloor (echo intensity data suggest that the wake can even reach the surface), and by inclinations of the bottom nepheloïd layer (as deduced from differences in echo intensities from beam to beam). Our analysis is validated by consistent relationships between the horizontal current direction and speed on one side and the characteristics of both dynamic (vertical velocity) and non-dynamic (echo intensity) parameters on the other. It is in good agreement with the simulations from a numerical model, and hence specifies the sensitivity (especially with respect to echo intensity) and accuracy of an instrument usually operated within fields of current and scatterers not disturbed by the device supporting it. In addition, the error velocity parameter displays specific characteristics that easily specify the thickness of the layer disturbed by the observatory, thus providing a technique to validate the quality of data acquired in similar conditions.

**Key words** *ADCP sensitivity – current lines inclination – observatory's wake*

## 1. Introduction

ADCPs have now proven their capabilities to sample phenomena ranging from surface waves, to small-scale internal waves, to mesoscale eddies and to general circulation. However, ADCPs are generally operated in current fields that can be assumed as homogeneous at a given level and at beam-spacing scale; hence, they generally work at best, which does not reveal their utmost performances. As shown hereafter, less favourable conditions, for instance when a relatively huge structure prevents from having a homogeneous mean current field around it, reveal unexpected aspects of their performances.

The GEOSTAR group has developed a prototype observatory aimed at being deployed with a carrier as deep as ~6000 m mainly to study geophysical phenomena (Beranzoli *et al.*, 2000, fig. 1). The observatory is a three-ton, semi-cubic (2.5×2.5×1.0 m$^3$) structure on which is set, among other oceanographical and geophysical instruments (CTD, seismometer, gravimeter, etc.), a 300-kHz ADCP (Workhorse Sentinel from RD Instruments) whose beams (20° angle) are unobstructed by the docking/undocking tetrahedral armature on top of the observatory. This relatively short-range (~150 m) ADCP was set instead of the long-range (~500 m, 75 kHz) initially planned because of funding cuts, even though the observatory is obviously too massive to allow the accurate study of near-bottom dy-

*Mailing adress*: Dr. Claude Millot, Laboratoire d'Océanographie et de Biogéochimie (LOB), BP 330, F-83507 La Seyne-sur-Mer, France; e-mail: cmillot@ifremer.fr

namic phenomena. Although wake disturbances induced on the near current field by such an observatory were anticipated, we did not expect the ADCP to be able to specify them and only expected to get data noisier than usual.

During a three-week test, from August 13 to September 1, 1998, at a depth of ~42 m in the Northern Adriatic sub-basin, eastern basin of the Mediterranean Sea, the ADCP was checked for oceanographic purposes (since we did not imag-

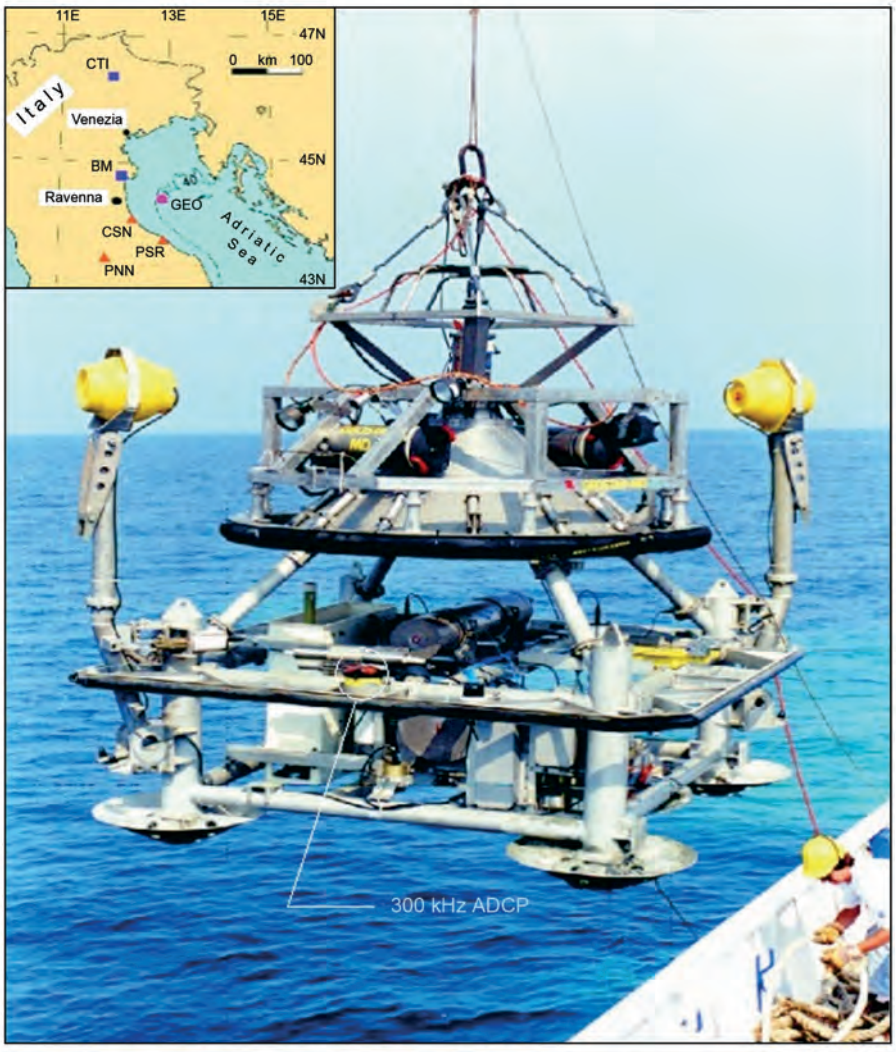


**Fig. 1.** The GEOSTAR Observatory during deployment. The conical upper part, the base of which is protected by a black rubber fender, is the mobile docker that is removed when the observatory is set on the bottom; it masks the upper part of the docking/undocking tetrahedral armature. Then, the docker is used only for recovery, hence as a female, to clamp the observatory via a pin system set on top of the four inclined tubes. The two vertical arms terminated by yellow spheres that contain magnetometers will be lowered on the bottom, *i.e.* away from the observatory. During the experiment, the ADCP is thus nearly on top of the observatory. Also shown is the deployment location.

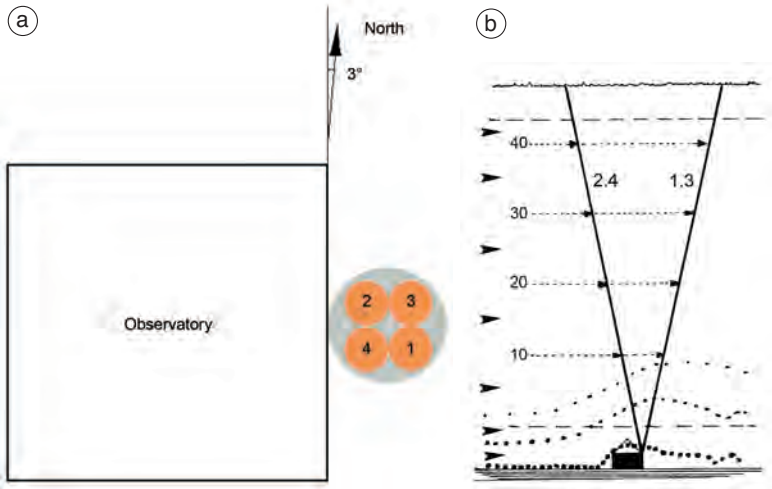


**Fig. 2a,b.** a) Actual orientation of the ADCP with respect to the observatory and magnetic north. b) Beams configuration and tens of cell numbers as seen when looking towards north; the upper and lower blank zones are delimited by dashed lines; the arrows represent an homogeneous current flowing towards east while the dotted lines schematise the current lines close to the bottom, and thus the structure (in both shape and concentration of suspended particles) of the nepheloïd layer as disturbed by the observatory.

ine being able to specify the wake disturbance). Hence, it was set to record Earth co-ordinates velocities calculated from 200 pings evenly transmitted during 10 min every hour (were it operated to specify the wake disturbances around the observatory, it would have been set to record single-ping values). Figure 2a specifies the beams numbers and the orientation of the ADCP with respect to the observatory and to magnetic north; the ADCP axis was roughly vertical (pitch and roll ~0.2°). Profiles were set to 50 cells 80 cm thick. Due to the ADCP location and to the blank zone, cell #1 was ~4.4 m above seafloor (asf). Due to the secondary lobe reflection on the sea surface, data are available up to a depth of ~5 m (cell #42). Figure 2b provides a sketch of the general experimental conditions.

The overall circulation in the study area is usually thought to be southwards along the large-scale isobaths (Orlic *et al.*, 1992). The circulation encountered during the experiment in the deep layer below the seasonal pycnocline, as illustrated by the progressive vector diagrams from cells #1-30 (fig. 3), was thus unexpected and rather complex. Diagrams from cells #31-42 are

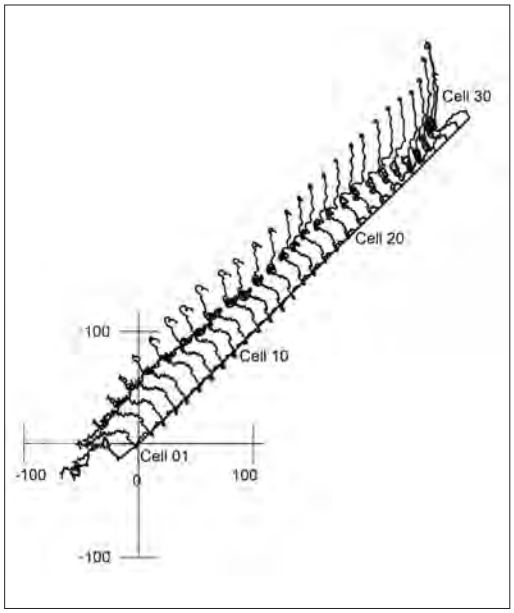


**Fig. 3.** Progressive vector diagrams from cells #1-30 plotted with respect to north (upwards) and with a 100-km scale.

markedly different from long-term ones too, and from the deeper ones since they were always in the surface mixed layer; hence, they are not plotted for clarity. Most of the variability shown by fig. 3 comes from tidal and inertial oscillations that induced relatively intense currents towards nearly all directions.

As indicated by vertical profiles from a ship-handled transmissometer operated at the beginning and end of the experiment and the time series from a transmissometer mounted on the observatory, a bottom nepheloïd layer several metres thick was present in permanence during the experiment. However, for sake of simplicity, we just consider hereafter that the concentration in suspended sediments decreases upwards. As schematised in fig. 2b, this layer is obviously uplifted by the station; just above the ADCP, one can thus easily expect that the layer will generally be inclined, so that echo intensity must differ from beam to beam in a way related to the current direction and speed.

These expected characteristics of dynamic (vertical velocity) and non-dynamic (echo intensity) parameters will be analysed thoroughly. In addition, we have analysed the error velocity parameter that represents the heterogeneity of both horizontal currents and the sums of beam-paired vertical velocities. We show that the error velocity distribution displays characteristics that allow specifying the depth range over which the current field is made significantly heterogeneous by the observatory or by a similar bottom irregularity. We thus provide criteria to check the current homogeneity, hence to validate bottom ADCP measurements.

To understand the data analysis in an easier way, the current field around the observatory simulated with a numerical model is described first (Section 2). ADCP characteristics and the speed data screening steps are presented in Section 3. The dynamic and non-dynamic data as well as the error velocity parameter are analysed in Sections 4 and 5, respectively.

## 2. The numerical current field around the observatory

Numerical simulations of the current field around the observatory were performed using the commercial CFD (Computational Fluid Dy-

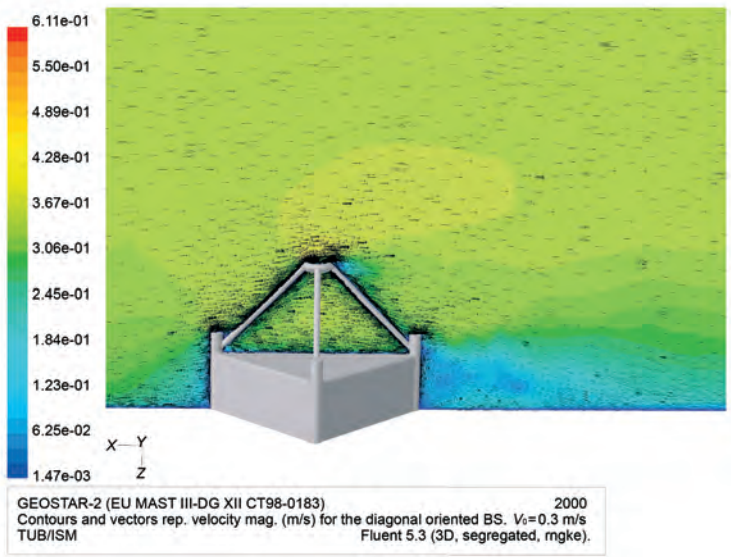


**Fig. 4a.** 2D current in a plane through the centre of the observatory with a far-field speed of 300 mm/s along a diagonal. Note that current is coming from the left.

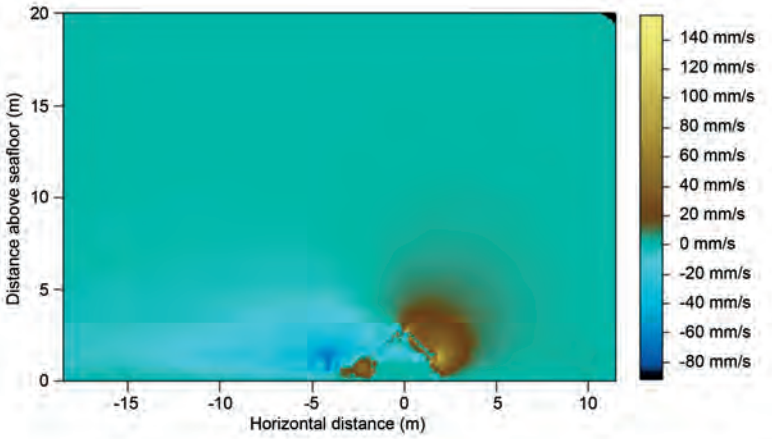


**Fig. 4b.** Vertical velocity in a plane through the centre of the observatory with a far-field speed of 300 mm/s along a diagonal. Note that current is coming from the right.

namics) software Fluent (2000). The effect of turbulence was considered by means of the RNG (Re-Normalization-Group) code for a $\kappa$-$\varepsilon$ model derived from the instantaneous Navier-Stokes equations. The analytical derivation results in a model with constants different from those in the standard $\kappa$-$\varepsilon$ model, and additional terms and functions in the transport equations for $\kappa$ and $\varepsilon$. The near-wall layer was approximated by a standard logarithmic function approach. The observatory was schematised by a block of 2.5×2.5×1.0 $m^3$ and by the 4 booms of the docking/undocking frame on top, which gives a total height of ~2.7 m asf.

Several sets of experiments were performed: two values of the mean speed (100 and 300 mm/s), two configurations for the observatory orientation (mean current parallel to a side or to a diagonal) and two domains (30 m/$x$ – direction of the mean current –, 20 m/$y$ and 20 m/$z$; 45 m/$x$, 20 m/$y$ and 40 m/$z$) were investigated. Parameters were adjusted (*i.e.* seafloor roughness down to 0) to obtain vertical velocity values as large as possible (*i.e.* more similar to the observed ones). Although the simulated vertical velocities were still lower than the observed ones, they reached the surface, consistently with the measured echo intensity data.

The results illustrated in fig. 4a,b represent the smaller domain (to provide more visible details of the current field around the observatory) and a mean current of 300 mm/s parallel to a diagonal. Although the ADCP is then located at ±~1 m from the observatory centre in both $x$ and $y$, simulations are considered in a vertical plane through the centre of the observatory. Although the current vectors at some distance from the observatory do not seem in fig. 4a to be strongly modified (due to the large difference between the vertical and horizontal components), significant vertical velocities are in fact induced over the whole water depth (fig. 4b). Maximum vertical velocity values that can be compared with those from the ADCP, *i.e.* at ~4-5 m asf (cell #1), reach ~10 mm/s, when values of ~1 mm/s are still encountered at ~15 m asf. Slopes of the simulated current lines (*i.e.* lines of iso-concentration in suspended sediments) are thus maximum (~1/30) at ~4-5 m asf. There, they correspond to a difference in depth along two opposite beams of ~6 cm that is much lower than the cell size (80 cm), and thus *a priori* hard to be shown. This is *a fortiori* valid for the upper cells since $W$ decreases more rapidly than the beam separation.

## 3. The ADCP data processing

To verify the basic assumption for ADCP technique, the 3D current field must be homoge-

neous horizontally, *i.e.* over ~2 m for cell #1 and ~15 m for cell #40. From the four beam velocities, each pair of opposite transducers (1-2 and 3-4) gives one horizontal and one vertical components. The two horizontal components are directly associated with *U* and *V*. With a homogeneous current field, the two vertical components ($W_{12}$ and $W_{34}$) are identical; hence, the 3D current profile is defined with some redundancy. Practically, a mean vertical velocity $W=(W_{12}+W_{34})/2$ is computed, as well as an error velocity $EV=C\cdot(W_{34}-W_{12})$ where $C=1/(\mathrm{sqrt}(2).\tan(20°))$ is a normalisation constant (RDI Technical Booklet, 1998). Another parameter to deal with is the echo intensity (*EIb* in dB) for each beam (#b) and cell, which represents the amount of energy echoed at given distances.

The Workhorse Sentinel model uses the broadband method based on the propagation delay computed from correlation between one ping and its echo (Gordon, 1996). In fact, single-ping beam velocities are generally not accurate enough so that ensemble-averages are performed (we used 200 pings emitted during 10 min every hour). In the Earth-coordinates mode, and for each single ping, there are three kinds of screening on velocity data: the correlation test, the fish rejection algorithm and the error velocity test.

The correlation test compares the correlation level and results to thresholds. Beam velocities either associated with a poor signal-to-noise ratio (that occurs in waters too much depleted in scatterers) or larger than a pre-defined ambiguity velocity are rejected. These problems were not often encountered.

The fish rejection algorithm detects an abnormal beam velocity for a specific cell or an echo much greater from one beam than from the others, which would make the strong echo from the «fishy» beam heard by the others, and the same velocity computed for all beams. The large concentration and gradient of suspended particles in the bottom nepheloïd layer, and the sometimes-large inclination of this layer, often led to such problems. In some cases, more than 80% of single-ping beam velocities were rejected.

In a heterogeneous current field, $W_{12}$ and $W_{34}$ are markedly different in general, so that *EV* is large. This often occurred for the lower cells, resulting in uncertainties larger than usual on the horizontal components. However, it is «frustrating» to eliminate all horizontal current values associated with an *EV* larger than a threshold, and not convenient to have gaps in a time series (*i.e.* for a given cell; we used the option «3-and-4-beam solution»). An analysis of the *EV* characteristics will show that it is possible to appreciate, in a statistical way, the thickness of the layer significantly disturbed by such an observatory.

## 4. The ADCP data analysis

### 4.1. *The dynamic parameters*

Up to 15-20-m asf, *W* (fig. 5) reached relatively large upward values (up to 40-50 mm/s) when *EV* (fig. 5) displayed variations that were similar both in time and on the vertical. The similarity between large *W* (*i.e.* large $W_{12}+W_{34}$) and large *EV* (*i.e.* markedly different $W_{12}$ and $W_{34}$) is consistent with what was expected.

The relationship between *W* and the horizontal current speed $M=[U^2+V^2]^{1/2}$ is also noteworthy. The regression lines for some specific cells and all directions (fig. 6) indicate that $W\sim0$ when $M=0$ everywhere, that *W* increases with *M*, and that this increase diminishes with the cell number (*i.e.* distance from the observatory). For cells numbers >15, *W* values are relatively small and no more depend on *M*. These features are consistent with the deformation of the schematised (fig. 2b) and simulated (fig. 4) current field.

Simulated *W*'s can also be compared with the measured ones (fig. 7). Obviously, the measured *W*'s are more scattered than the simulated ones, due to the ranges in both speed and direction of the *in situ* currents, and to the inaccuracies in the *W* computations, especially those due to the heterogeneity of the current field. Therefore, only mean measured *W*'s were plotted, hence showing that they are ~3 times larger than the simulated ones. However, the mean curves have a roughly similar shape and they all reach ~0 at ~20 m asf. We are unable to specify which kind of curves is the most realistic one. Furthermore, vertical velocities are in fact induced up to the surface, as shown hereafter (although not just above the observatory, *i.e.* non-measurable by the ADCP and not in the domain considered

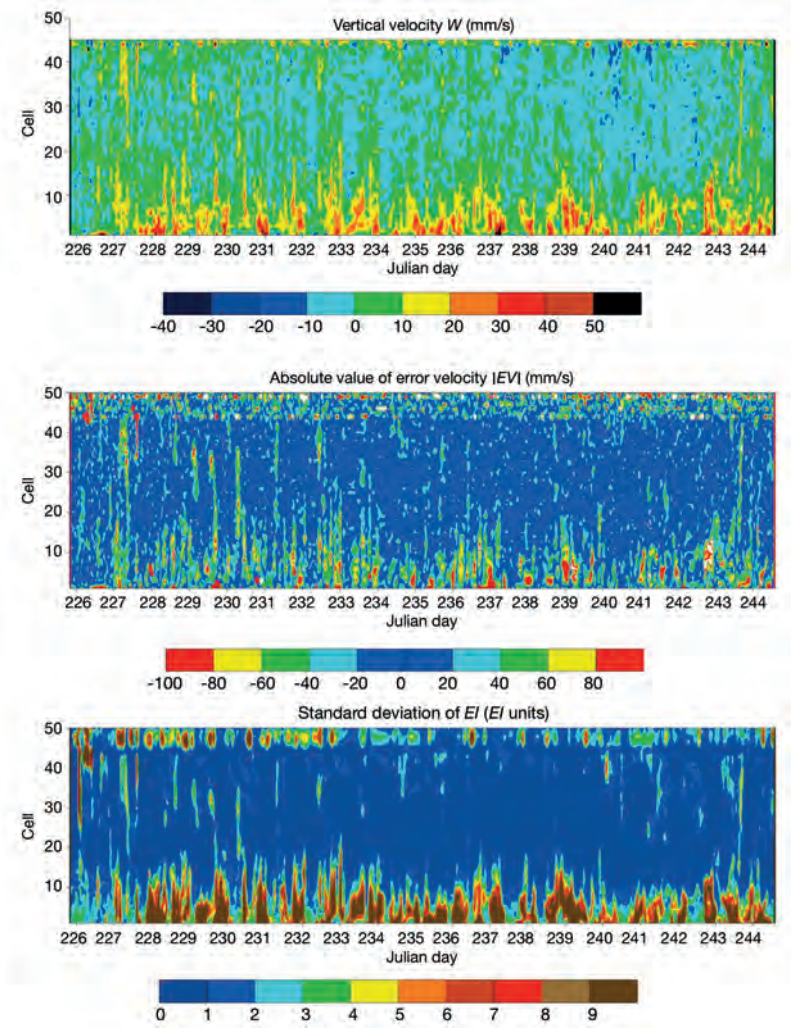


**Fig. 5.** Vertical velocity *W* (up), absolute value of the error velocity *EV* (middle) and standard deviation of the echo intensity *EI* in arbitrary units (down) as a function of depth (*i.e.* cells #) and time (Julian days).

for the simulations). Since inaccuracy in *W* computation does not necessarily mean large *W*, we are tempted to think that measured *W*s are, on average, more realistic than simulated *W*s.

## 4.2. *The non-dynamic parameters*

As schematised in figs. 2b and 4a,b, the nepheloïd layer being uplifted and inclined should induce a marked heterogeneity in the echo intensity *EIb* along every beam and for every cell. In the open sea, *EIb* mainly provides information on the amount and distribution of zooplankton. In the present case, this information mainly concerns i) the zooplankton diurnal migration on the vertical, and ii) the concentration and thickness of the bottom nepheloïd layer above the observatory, which partially depends on the current speed and direction. Plots

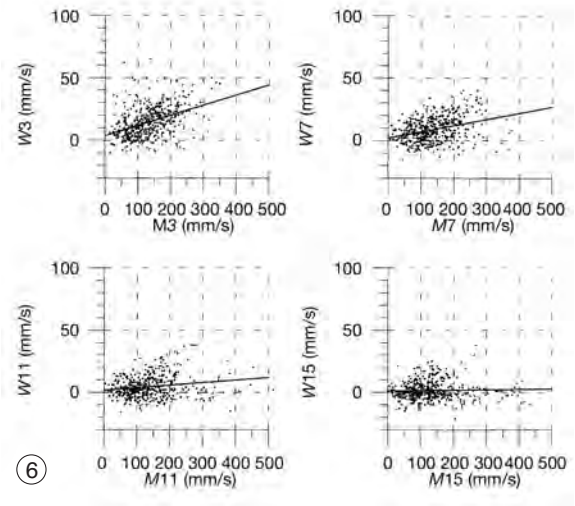


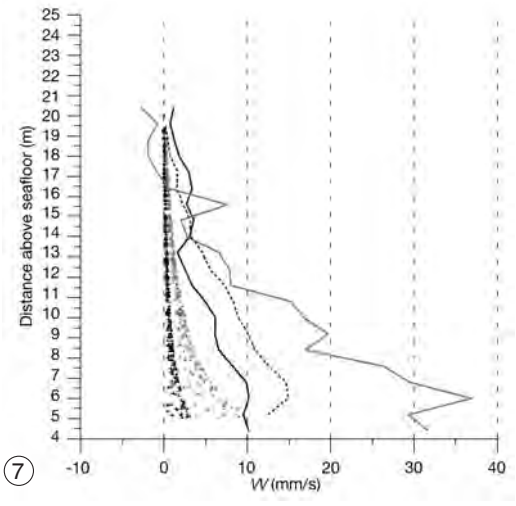


**Fig. 6.** Relationships and linear regression lines between *W* and the current speed *M* (in mm/s) for cells #3, 7, 11 and 15 (*i.e.* at 6, 9.2, 12.4 and 15.6 m above the bottom).

**Fig. 7.** Simulated *W*s (+) for mean currents of 100 (black) and 300 (red) mm/s parallel to a diagonal are those obtained in a prism centred on the observatory and having a 4-m side at ~20 m asf. To get a sufficient number of measured *W*s to compare with, we considered altogether currents towards sectors of 45° roughly aligned with the diagonals (~45°, 135°, 225° and 315°) and in the ranges of 80-120 mm/s (solid black) and 250-350 mm/s (solid red). Since measured values are much more scattered than simulated ones, we just reported the corresponding averaged profiles. The blue dashed line represents the averaged *W*s whatever the mean current direction and module.

of the measured *EIb versus* depth *versus* time (not shown) thus depend on several phenomena and are not clearly instructive.

It can be assumed that «natural» *EIb* variations (due to both the nepheloïd layer *per se* – *i.e.* undisturbed by the observatory – and the zooplankton vertical migrations) are horizontally homogeneous. In order to eliminate them, we consider *EIb* variations along a specific beam relatively to variations along the other beams (*EIb*s must first be normalised since transducers are not of equal quality). Figure 8 illustrates, for the 4 beams (b), the difference *DIb* between a given *EIb* and the average over the 3 other *EIb*s as a function of the current direction (north is upward) and depth (represented by the cell #1-42). *DIb* thus represents relative echo intensity.

Mainly for cells close to the observatory (cells #1-15) and for upper cells, a specific *DIb* appears to be larger or lower than the others depending on the current direction. For instance, *DI*4 is relatively large when the current is directed towards south to west. For most cells, this corresponds to a nepheloïd layer denser along beam #4 than along the other beams above the observatory. As expected from figs. 2a,b and 4a,b, the nepheloïd layer is higher along beam #4 than along the other beams for currents towards south to west. Similar features occur for the other beams. The analysis of relative echo intensity signals thus allows showing slopes of the bottom nepheloïd layer that were not thought, according to simulation, to be measurable.

Especially for *DI*4 and *DI*2, large values are encountered over the whole water depth (~42 m), hence showing that the wake of the observatory sometimes reached the surface, thus probably inducing changes in particles concentration, *i.e.* in colour, at the surface, eventually downstream from the zone sampled by the ADCP. The reverse (*DIb* relatively low) occurs, for all beams, in the opposed and perpendicular directions (*i.e.* where one of the others *DIb*s is relatively large). Also to be noticed is that the negative parts of *DI*2 and

*DI*4 are more negative than those of *DI*1 and *DI*3. These asymmetrical features are related to the fact that more beams are in the wake of the observatory (*i.e. EIb*s are more similar and *DIb*s are lower) when the current is towards east than when it is towards west. This is due to the fact that the ADCP is located on the eastern side of the observatory and is consistent with the distribution of the data computed from either 4 beams (*P*4) or 3 beams only (*P*1) as indicated in fig. 9a-c for a

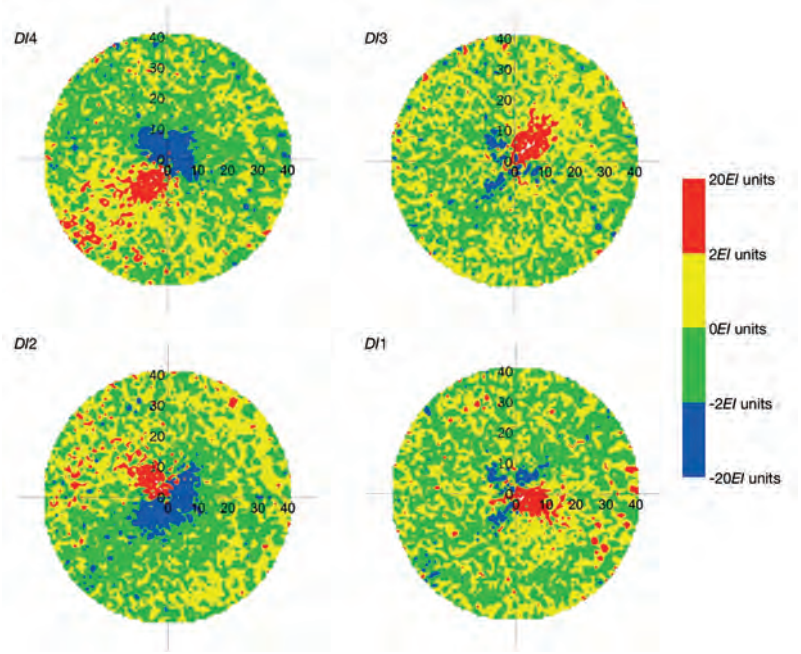


**Fig. 8.** Differences *DIb* between the normalised *EIb* and the average over the 3 other *EIb*s *versus* the current direction (north is upward) and cell number. The diagrams can be analysed as if the observatory were in between them.

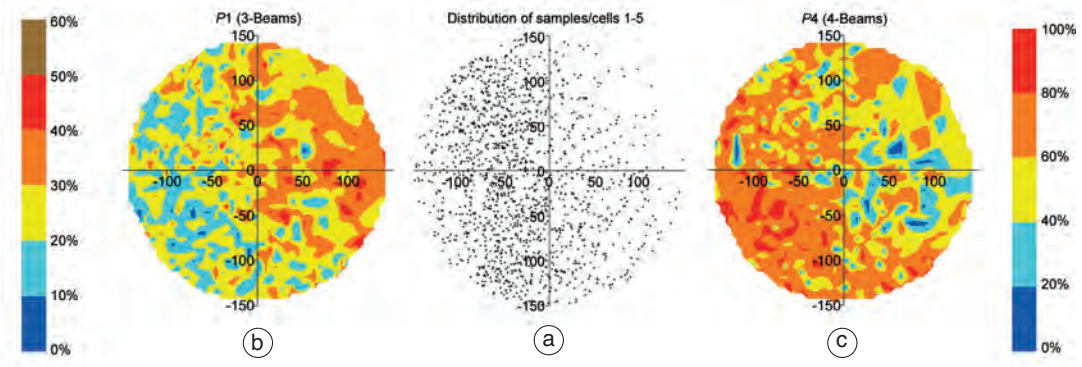


**Fig. 9a-c.** a) Distribution of samples for cells #1-5 as a function of the current direction and speed up to 150 mm/s (north is upward). b) Distribution of the percentage of data computed from 3 beams only (*P*1) and corresponding scale. c) Distribution of the percentage of data computed from 4 beams (*P*4) and corresponding scale.

given cell (#15). Indeed, more data are computed from the 4 beams when the current is towards west, hence not strongly disturbed above the ADCP, than when it is towards east, hence the ADCP being in the wake of the observatory. It can thus be concluded that: i) the wake induced by the observatory can extend several tens of metres above it, and ii) the slightly out of centre location of the ADCP (~1 m) is consistently reflected on the wake signature (over several tens of metres).

The concentration in particles within the nepheloïd layer *per se* increases downwards and varies with time. Hence, it is impossible (without any measurement in distance to the observatory) to identify and separate the influences, on the *DIb*s, of either the concentration in particles or the inclination of the nepheloïd layer. In order to deal with a somehow synthetic parameter representative of the *EIb*s heterogeneity, we computed, for each cell and over time, the *EIb* standard deviation $[1/4 \cdot \Sigma_b(EIb - EIm)^2]^{1/2}$, whereas *EIm* is the average of the *EIb*s over *b*. It is clear that the *EIb* standard deviation (fig. 5c) and *W* (fig. 5a) have very similar distributions**,** especially in the 15-20-m bottom layer where both can be large. This direct correspondence between *a priori* independent (one non-dynamic and one dynamic) parameters clearly validates fig. 2a and 4a,b and shows that the larger the inclination of the nepheloïd layer, the larger the vertical velocity.

It must be emphasised that the *EIb* standard deviation, and consequently the inclination of the surfaces of equal concentration in suspended particles, is computed from differences between *EIb*'s in cells that are separated horizontally by a few metres only (*e.g.*, ~2 m for cell #1 and ~15m

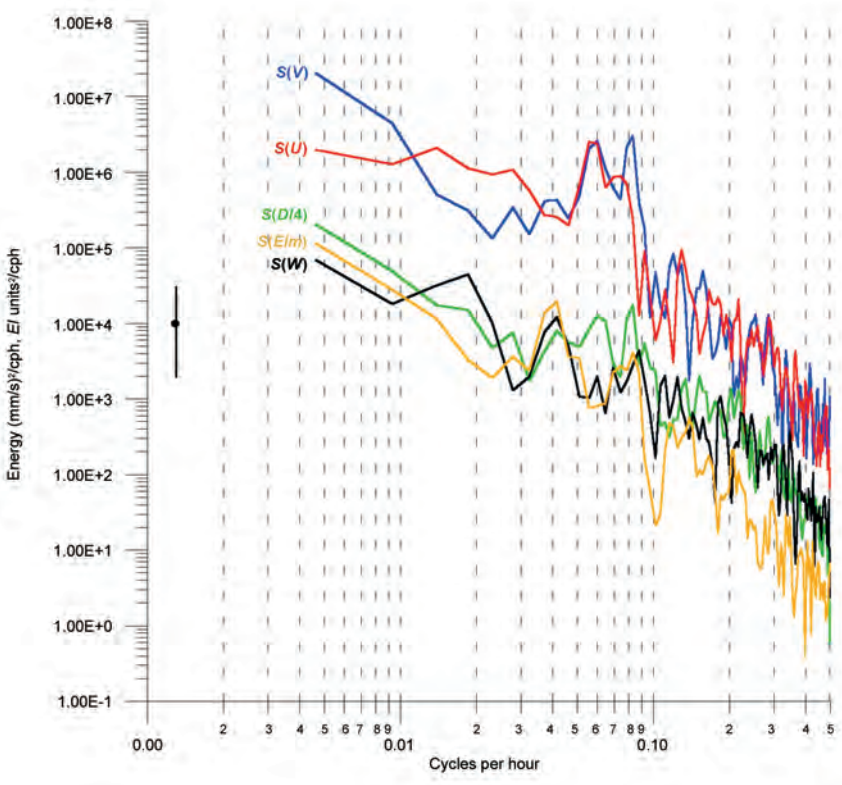


**Fig. 10.** Spectra of *U* (red), *V* (blue), *W* (black), *EIm* (orange) and *DI*4 (green) at cell #5 averaged over 2 pieces to give 4° of freedom. The confidence interval is the 90% one.

for cell #40). Whatever the current field homogeneity is, and thus whatever the quality of the current computations, this analysis demonstrates that the echo intensity is a very sensitive signal that provides significant information (not perceptible with a homogeneous current field).

### 4.3. *Spectral analysis*

Figure 10 displays dynamic (*U*, *V*, *W*) and non-dynamic (*EIm*, *DI*4) parameters spectra at cell #5 (representative of the 15-20-m bottom layer). Classically, the *U* and *V* spectra show a similar amount of energy at the inertial frequency (clockwise-polarised circular oscillation at ~0.06 cph) while the semidiurnal (~0.08 cph) and diurnal (~0.04 cph) frequencies are shown mainly on the *V* spectrum (north-south rectilinear currents in the Northern Adriatic). Since *EIm* and *W* are purely integrated (over beams) parameters, they do not change markedly according to a circularly polarised current (the inertial frequency will not appear on the spectra) while they change according to a rectilinear current (at twice the corresponding tidal frequency). Both *EIm* and *W* are also sensitive to the zooplankton diurnal migration, which is not a purely diurnal signal so that energy is also introduced at the semidiurnal frequency (and higher harmonics as well). Therefore, the fact that only tidal frequencies, *i.e.* not the inertial frequency, are shown on both *EIm* and *W* is consistent with our analysis.

In addition, all peaks (diurnal, inertial, semidiurnal) must appear on the spectrum of a parameter such as *DI*4 (insensitive to zooplankton diurnal migration) since tidal currents and inertial currents induce an inclination of the nepheloïd layer at corresponding frequencies. As shown by fig. 10, a peak (at the inertial frequency) on the spectrum of a non-dynamic variable (*DI*4) coming from a purely dynamic phenomenon (the inertial oscillations) definitely validates our analysis.

## 5. More on the error velocity parameter

Theoretically, a homogeneous current field leads to an error velocity $EV=0$. Practically, $EV\neq 0$ indicates that the data are not accurate and/or that the current field is heterogeneous. Let us consider an ADCP suitably mounted (nearly centred) on a symmetrical (with respect to current direction) structure, and collecting data at best (in terms of *e.g.,* pings averaging). The analysis below shows that the *EV* characteristics allow specifying which cells are markedly influenced by the structure, hence validating the data from a statistical point of view.

With a heterogeneous current field, and for a given cell, *Ub* and *Wb* ($b=3, 4$) define the actual current components from beams 3 and 4, and *Vb* and *Wb* ($b=1, 2$) the actual current components from beams 1 and 2 (fig. 11a). *F* being the angle from the ADCP axis, the radial velocities *Rb* and the computed vertical velocities are (for more details see van Haren *et al.*, 1994)

$$R1=-V1\sin F-W1\cos F$$

$$R2=V2\sin F-W2\cos F$$

$$R3=-U3\sin F-W3\cos_S F$$

$$R4=U4\sin F-W4\cos F$$

$$W34=-(R3+R4)/2\cos F=-[(U4-U3)\tan F+ +(W3+W4)]/2$$

$$W12=-(R2+R1)/2\cos F=-[(V2-V1)\tan F+ +(W1+W2)]/2.$$

In case the actual current field is homogeneous, $U3=U4=U$, $W3=W4=W34$, $V2=V1=V$, and $W1=W2=W12$, with the consequence that the *U*-*V*-*W* field is specified with measurement inaccuracies that are quantified by $EV/C=(W34-W12)$. In case that the current field is heterogeneous, with $DU=U3-U4$ and $DV=V1-V2$, it results in

$$EV/C=(DU-DV)\tan F+(W3+W4)-(W1+W2).$$

Assuming a simplified cubic observatory oriented northwards (fig. 11b), and an ADCP located on its eastern side, two relationships can be expected. For currents of similar speed towards directions A and A′ that are symmetrical with respect to the east-west axis, identities between the *Ub* and *Vb* of both situations lead to $EV_A=-EV_{A'}$. For currents towards either east or west, $W2=W4$, $W1=W3$, $U3=V1$ and $U4=V2$; hence $EV=0$ (also obvious from the previous re-

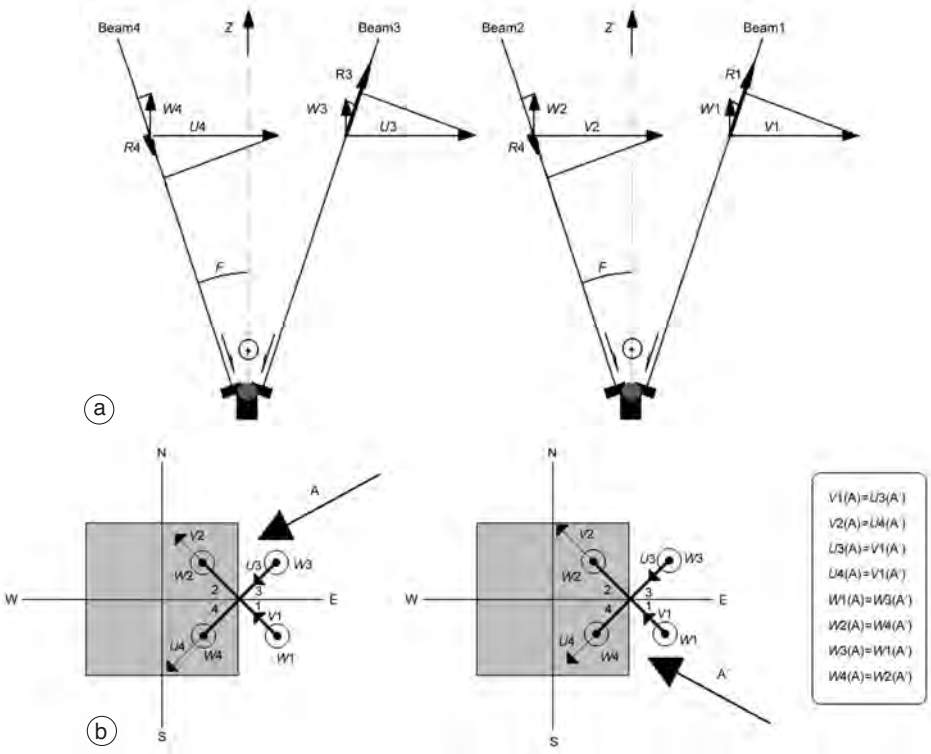


**Fig. 11a,b.** a) Beams and current components configuration in case of an heterogeneous current field; b) horizontal components of currents towards directions A and A′ symmetrical with respect to east-west, and components correspondence.

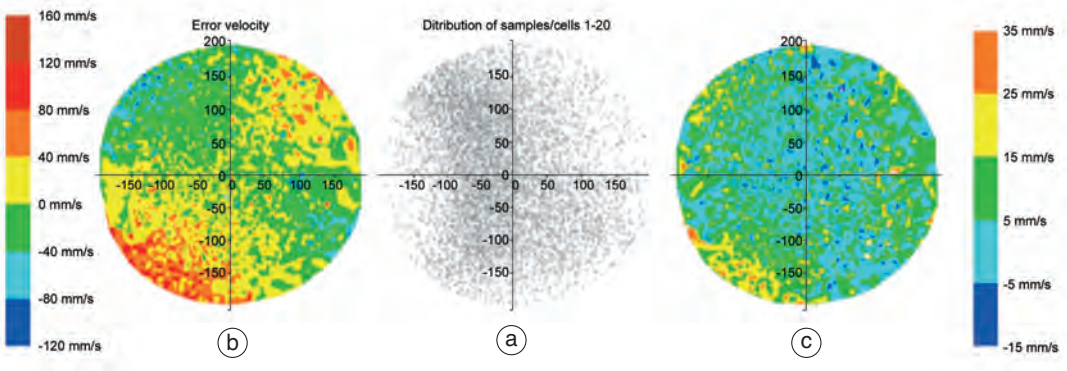


**Fig. 12a-c.** a) Distribution of samples for cells #1-20 as a function of the current direction and speed up to 200 mm/s (north is upward). b) Distribution of the error velocity (scale on the left) for cells #1-20 *versus* current direction and speed. This diagram displays neither the number of samples (shown in a) in a specific area of the diagram, nor the variance in that specific area. The error values that are indicated are interpolated from the errors associated with each sample, so that errors for areas with few samples are less significant. c) The same for the vertical velocity (scale on the right).

lationship). If the ADCP were centred, EV would have been = 0 for currents towards either north and south, and $EV_A = EV_{-A}$ for currents towards opposed directions (A and −A). In a given data set, any indication of such relationships will account for a significant heterogeneity of the current field. Conversely, if *EV* does not display any specific distribution (*i.e.* is only noisy), the current field can be considered homogeneous. Considering these relationships over depth can specify, from a statistical point of view, the thickness of a significant wake disturbance.

Verifying these *EV* specific relationships with our data set can be hampered by the fact that both the speed and the direction are not homogeneously distributed. To get a distribution as homogeneous as possible, we considered all couples speed-direction from cells #1-20 for the whole experiment (fig. 12a) and their associated EV (fig. 12b) and W (fig. 12c) values. We have neglected the difference between north and the 3° actual orientation. Figure 12b shows that, whatever the horizontal speed is, the *EV* sign changes when crossing the east-west axis, which validates the corresponding theoretical relationship ($EV = 0$) for currents towards east or west. Also, for all directions and speeds, the theoretical relationship $EV_A = -EV_{A'}$ is clearly validated. To be noticed is the (sole) other sign change near directions towards southeast and northeast, *i.e.* the north-south axis is clearly not a symmetry axis as would have been the case for a ADCP located in the centre of the observatory. In such a case, the relationships ($EV = 0$ for north and south directions, and $EV_A = EV_{-A}$ or opposed directions) are clearly not validated. Therefore, the *EV* distribution in fig. 12b clearly shows that i) the current field is heterogeneous and ii) the ADCP is not centred.

Although the interpolation procedure is rough for very large speeds due to the low number of points, it can be considered that the larger/lower the speed, the larger/lower the *EV* absolute values. For what concerns *W*, most values are positive and, the larger the speed the larger *W*. Also, *W* values are larger for currents towards west than for currents towards east. These results are consistent with what was intuitively thought and previously demonstrated with the simulation (fig. 4b) and the data analysis (fig. 6).

It can thus be concluded that, in case heterogeneity of the current field is induced by some semi-cubic structure set on the bottom, the EV distribution actually displays those characteristics that are expected from the algorithms. Analysing this parameter's distribution can thus allow specifying the layer thickness modified by such a structure. Obviously, these remarks also apply to a structure set at intermediate depths and to the current field above and below it. They can also be extended to structures that are parallelepipedic and currents that are symmetric with respect to the ADCP location.

## 6. Conclusions

A 300-kHz ADCP set on a semi-cubic (2.5× ×2.5×1.0 $m^3$) bottom observatory has allowed specifying the wake disturbances induced on the current field.

With a far field general current of 20-40 cm/s, upward vertical velocities of 40-50 mm/s were computed in a 15-20-m bottom layer. Although these experimental values are noisier than usual, mainly due to the heterogeneity of the current field above the observatory, they are consistent with (although larger than) simulated values, and hence considered significant. In such conditions, the wake of the observatory can probably extend ~40 m above seafloor at least (even if not directly above the observatory).

Differences in echo intensities along the beams have demonstrated that surface of iso-concentration in suspended particles were inclined over the observatory, consistently with what was expected from the general current direction and speed.

The relationships between the horizontal current direction and speed on one side and the characteristics of both dynamic (vertical velocity) and non-dynamic (mean echo intensity as well as relative echo intensities along the beams) parameters on the other side are also consistent with the oscillatory character of mesoscale (*i.e.* inertial and tidal) currents. Indeed, spectral characteristics expected for all these parameters, in association with currents polarised at the inertial frequency as well as with rectilinear currents at diurnal and semidiurnal frequencies, are clearly retrieved.

Finally, we have shown that the error velocity parameter displays specific characteristics that specify the thickness of the layer disturbed by such a semi-cubic observatory from a statistical point of view. This parameter can thus be used to check the validity of ADCP data collected in such a way, hence providing a criterion for qualifying this or that time series.

More generally, our analysis demonstrates how sensitive (especially for what concerns echo intensity) and accurate is an instrument usually operated in more favourable conditions (such as on a mooring line or directly on the bottom with a profiled mooring frame), which does not allow its utmost performances to be appreciated.

Considering the importance of induced vertical velocities compared to that of undisturbed horizontal currents (up to $O(10^{-1})$ within a depth range corresponding to a few times the observatory height), such a massive observatory is obviously not adequate to study finely currents close to the bottom. Such an observatory can efficiently host long range ADCPs devoted to the study of the general circulation and of mesoscale processes within bottom layers several 100s-m thick.

## Acknowledgements

The GEOSTAR group has been supported by EU (grants MAS3-CT95-0007 and MAS3-CT98-0183).

*REFERENCES*

BERANZOLI, L., T. BRAUN, M. CALCARA, D. CALORE, R. CAMPACI, J.-M. COUDEVILLE, A. DE SANTIS, G. ETIOPE, P. FAVALI, F. FRUGONI, J.-L. FUDA, F. GAMBERI, F. GASPARONI, H.W. GERBER, M. MARANI, J. MARVALDI, C. MILLOT, P. PALONGIO, G. ROMEO and G. SMRIGLIO (2000): European seafloor observatory offers new possibilities for deep-sea study, *Eos, Trans. Am. Geophys. Un.*, **81** (5), 45-49.

FLUENT (2000): *CFD Software, Online Manuals* (Fluent Germany GmbH, Darmstadt).

GORDON, R.L. (1996): *Acoustic Doppler Current Profilers. Principles of Operation: a Practical Primer* (RD Instruments Publication), 2nd edition for broadband ADCPs.

ORLIC, M., M. GACIC and P. LA VIOLETTE (1992): The currents and circulation of the Adriatic Sea, *Oceanol. Acta*, **15** (2), 109-124.

RDI TECHNICAL BOOKLET (1998): *ADCP Coordinate Transformation; Formulas and Calculations* (RD Instruments Publication).

VAN HAREN, H., N. OAKEY and C. GARRETT (1994): Measurements of internal wave band eddy fluxes above a sloping bottom, *J. Mar. Res.*, **52**, 909-946.